Bandgap Tailoring via Si Doping in Inverse-Garnet $Mg_3Y_2Ge_3O_{12}$:Ce^{3+} Persistent Phosphor Potentially Applicable in AC-LED

Hang Lin,[†,‡] Ju Xu,[†,‡] Qingming Huang,[§] Bo Wang,[†] Hui Chen,[†] Zebin Lin,[†] and Yuansheng Wang[*,†,‡]

[†]Key Laboratory of Design and Assembly of Functional Nanostructures, Fujian Institute of Research on the Structure of Matter, Chinese Academy of Sciences, Fuzhou, Fujian 350002, People's Republic of China

[‡]Fujian Provincial Key Laboratory of Nanomaterials, Fuzhou, Fujian 350002, People's Republic of China

[§]Instrumentation Analysis and Research Center, Fuzhou University, Fuzhou, Fujian 350002, People's Republic of China

Ⓢ Supporting Information
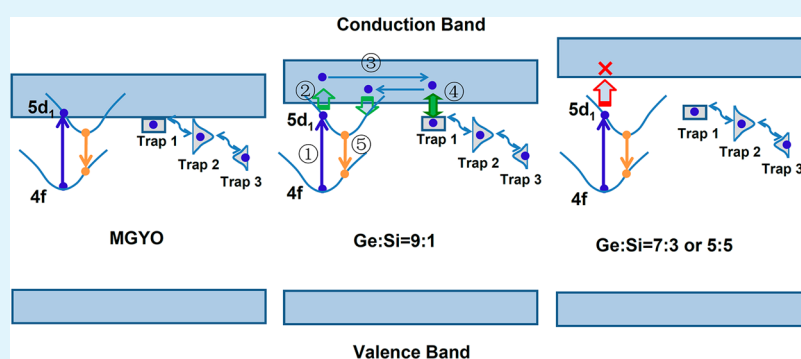
ABSTRACT: The state-of-the-art alternating-current light-emitting diode (AC-LED) technique suffers from adverse lighting flicker during each AC cycle. Aiming to compensate the dimming time of AC-LED, herein, we report a novel $Mg_3Y_2(Ge_{1-x}Si_x)_3O_{12}$:$Ce^{3+}$ inverse-garnet persistent phosphor whose afterglow is efficiently activated by blue light with persistent luminescence in millisecond range. It is experimentally demonstrated that Si doping tailors the host bandgap, so that both the electron charging and detrapping in the persistent luminescence process are optimized. To explore the origin of the millisecond afterglow, we performed a series of thermoluminescence analyses, revealing three types of continuously distributed traps in the host. Finally, an AC-LED prototype device was fabricated, which exhibits the warm white emission with a reduced percent flicker of 71.7%. These results demonstrate that the newly developed persistent phosphor might be a promising candidate applicable in low flickering AC-LED which has advantages of cheaper price, longer lifetime, and higher energy utilization efficiency.

KEYWORDS: LED, persistent luminescence, trap, flicker effect, phosphors

1. INTRODUCTION

With the advent of LEDs-based solid-state lighting, a revolution that is fast approaching will make our life more sustainable. At present, the mainstream product dominating commercial LED market is DC-LED driven by direct current flowing in a forward direction to allow electron–hole recombination in $p–n$ junction. Thereupon, the input 110 V/220 V alternating current (AC) from the city power should be converted to DC for driving the LED module.[1−3] During the AC to DC conversion, there is ∼30% unnecessary electric power consumption;[4,5] furthermore the generated massive heat would result in yellowing of the encapsulated organic resins and degradation of the embedded phosphors.[6−8] The required current rectifiers (or switching power supplies) and constant current sources increase the cost and complicate the product appearance and design; and, more important, the lifetime of the capacitor series in AC/DC converter is limited to ∼20 000 h, which is much shorter than that of the blue chip (∼1 million hours).[9,10] Recently, to overcome these shortcomings of DC-LEDs, more attention has been paid to AC-LEDs in both the industrial and academic circles, owing to their tremendous merits of not only lower price (thanking to the reduced redundant electronic components) but also higher energy utilization efficiency, more compacted volume, and longer service life.[9−14] However, a dimming time of 5−20 ms is unavoidable in every AC cycle,[9] resulting in a flicker effect that may induce photosensitive epilepsy, migraines, and headaches in certain people.[15] How to restrain the lighting flicker is the key issue for further developing the AC-LED technique.

Persistent luminescence (PersL), a phenomenon exhibiting emission of light after ending the excitation source, has aroused great interest for its wide applications in security signs, night
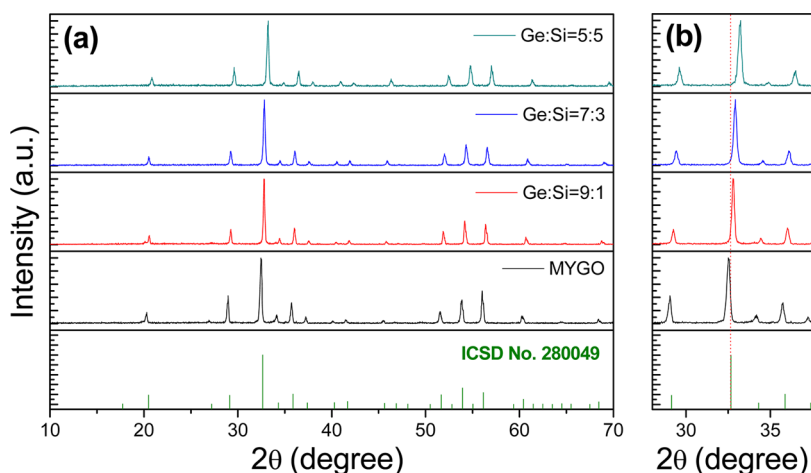
Figure 1. (a) XRD patterns of $Mg_3Y_{1.99}(Ge_{1-x}Si_x)_3O_{12}:0.01Ce^{3+}$ ($x = 0-0.5$) samples and the standard data of MYGO phase (ICSD No. 280049). (b) Magnified XRD patterns in the range of $28-38°$.

displays, optical storage media, vivo bioimaging, and so on.[16−21] For these applications, the longer persistent time is usually desired. In comparison, searching for persistent phosphors with short period phosphorescence, typically in the time range of millisecond, has received little attention. Garlick et al. first studied the UV excited short period phosphorescence during the first few milliseconds in $ZnS:Mn^{2+}$.[22] Kanai et al. observed the X-ray activated intense millisecond afterglow in the $(Gd_{2.908}Ce_{0.012})(Al_{0.56}Ga_{0.44})_{5.08}O_{12}$ crystal.[23] Recently, a novel and promising application of PersL materials in AC-LEDs was revealed, since the afterglow in millisecond range is hopefully applicable to compensate the dimming time in the AC cycle.[9−14] Liu and Chen et al. reported the feasibility of $SrSi_2O_2N_2:Eu^{2+},Mn^{2+}$, $SrAl_2O_4:Eu^{2+},Ce^{3+},Li^+$, and $SrAl_2O_4:Eu^{2+}$, R^{3+} (R = Y, Dy) green persistent phosphors for AC-LEDs.[9−11] Our group also developed a blue-light activated $Gd_{2.98}Al_2Ga_3O_{12}:0.02Ce^{3+}$ yellowish-green persistent phosphor that is able to reduce the percent flicker from 100% to 69%.[12] However, to date, there is still no appropriate guidance for design such special persistent phosphors, and the in-depth knowledge on the origin of the millisecond afterglow is lacking.

As known, PersL involves two basic processes: charging and detrapping. The electron charging proceeds with the aid of high radiation energy through promoting 4f electrons of the active rare earth ions (REI) to conduction band (CB) of the host.[18,24,25] The electron detrapping occurs by recombination of the electrons released from the traps with emissive centers.[26,27] To meet the requirements for AC-LED application, both of these processes need to be finely controlled. First, the charging wavelength should be adjusted to blue region to match with the commercial InGaN chip. Second, the detrapping should be very fast, and thus, the modulated trap depth ought to be shallow. From the design point of view, these goals can be achieved via a "bandgap engineering" strategy initially proposed by Ueda et al. when preparing the blue-light activated $Ln_3Al_{5-x}Ga_xO_{12}:Ce^{3+}$ (Ln = Y, Gd, Lu; $x = 1-4$) PersL ceramics.[28−31] On one hand, the energy gap between the blue-light excited level of REI and CB is optimized so that electron jumping to CB via photoionization is enabled,[28−32,12] while the electron retrapping, which seriously influences the PersL intensity, is avoided.[32] On the other hand, the trap with a specific energy depth located below CB becomes shallow, resulting in the shortening of the PersL lifetime and the

enhancement of the PersL intensity.[28] Worthy to be noted, such new bandgap engineering strategy for developing PersL materials has not yet been applied to the short-phosphorescent AC-LED phosphor.

In the present work, we systematically investigated the blue-light activated $Mg_3Y_2(Ge_{1-x}Si_x)_3O_{12}:Ce^{3+}$ ($x = 0-0.5$) inverse-garnet persistent phosphor for the first time. This material exhibits a fast decay in the millisecond time window. It is demonstrated that Si doping tailors the host bandgap, whereby the PersL lifetime and the PersL intensity are optimized. With the aid of thermo-luminescence technique, the electron detrapping process was revealed. Furthermore, the availability of this phosphor for compensating AC flicker was evaluated by coupling it with a commercial blue-chip. The fabricated AC-LED prototype device yields warm white light with a reduced percent flicker of 71.7%.

2. EXPERIMENTAL SECTION

$Mg_3Y_2(Ge_{1-x}Si_x)_3O_{12}:Ce^{3+}$ ($x = 0-0.5$) samples were synthesized by a high-temperature solid-state reaction using high-purity chemicals (Alfa) of Y_2O_3, MgO, GeO_2, SiO_2, and CeO_2 as starting materials and a small amount of H_3BO_3 as flux. A batch of about 2 g of the powders was weighed at the stoichiometric ratio and mixed and ground in an agate mortar for 30 min by adding some ethanol. Then, the mixture was dried, placed in an electric tube furnace, and sintered at 1350 °C for 4 h under 95% N_2+5% H_2 reductive atmosphere.

X-ray diffraction (XRD) patterns of the samples were collected using a powder diffractometer (Rigaku, Miniflex600) with a continuous scanning rate of 5°/min for phase determination and a step scanning rate being 8 s per step (step size, 0.02°) for Rietveld refinement. The photoluminescence (PL), photoluminescence excitation (PLE), persistent luminescence (PersL), persistent luminescence excitation (PersLE) spectra, and persistent decay curves were all measured by a FLS920 spectrophotometer (Edinburgh Instruments) with a 450 W xenon arc lamp as the light source. The quantum yield (QY) test was performed by using a barium sulfate coated integrating sphere attached to the spectrophotometer. For the themoluminescence (TL) measurements, the samples were mounted on a thermal stage (77−873 K, THMS600E, Linkam Scientific Instruments), exposed to 445 nm blue-light irradiation for 5 min at the setting temperature, and then heated to 573 K with a heating rate of 1 K/s. Meanwhile, the luminescent intensity variation of Ce^{3+} by monitoring at 580 nm was recorded by employing the kinetic mode of FLS920. The final TL curves were obtained by transforming the measured time dependent luminescent curves to the temperature dependent ones. The chromaticity parameters of the fabricated w-LEDs were measured

in an integrating sphere of 50 cm diameter connected to a CCD detector with an optical fiber (HAAS-2000, Everfine Photo-E-Info Co., Ltd.). The percent flicker of AC-LED was measured by a rapid recording photometer (Photo-2000F, Everfine Photo-E-Info Co., Ltd.) with a sampling rate of 20 kS/s.

3. RESULTS AND DISCUSSION

3.1. Microstructure Analyses. XRD patterns of $Mg_3Y_{1.99}(Ge_{1-x}Si_x)_3O_{12}$:0.01$Ce^{3+}$ (x = 0−0.5) samples are presented in Figure 1. All the diffraction peaks coincide well with the standard data of $Mg_3Y_2Ge_3O_{12}$ (ICSD No. 280049), with no appreciable signal from impurities when x < 0.5. For the $Mg_3Y_{1.99}Ge_3O_{12}$:0.01Ce^{3+} (MYGO:Ce^{3+}), the diffraction peaks deviate from the standard ones toward the lower 2θ side, caused by the substitution of Ce^{3+} (r_{Ce} = 1.14 Å) for Y^{3+} (r_Y = 1.02 Å). With increasing of Si content, XRD pattern gradually moves to the higher 2θ side probably ascribed to the lattice shrinkage induced by the replacement of Si (r = 0.42 Å) for Ge (r = 0.53 Å). To further explore the structure variation, XRD Rietveld refinement analysis (Figure 2a) was performed on an
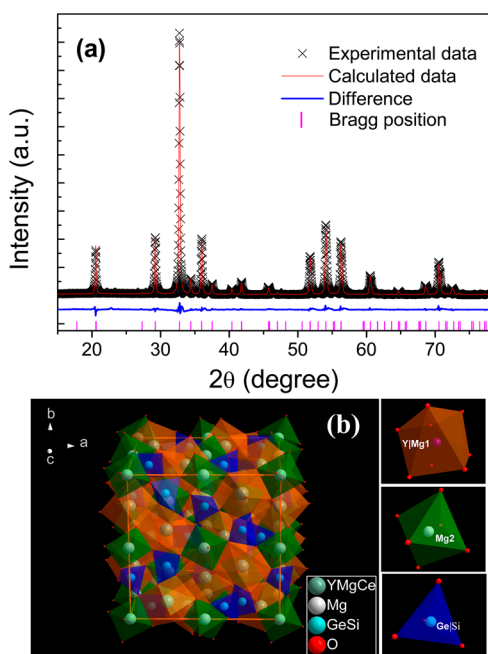

Figure 2. (a) XRD Rietveld refinement of the $Mg_3Y_{1.99}Ge_{2.7}Si_{0.3}O_{12}$:0.01$Ce^{3+}$ with the data and the fit represented by points and the line. (b) Crystal structure of $Mg_3Y_2Ge_{2.7}Si_{0.3}O_{12}$, showing coordination environment of Y, Mg, Ge, and Si.

exemplary $Mg_3Y_{1.99}Ge_{2.7}Si_{0.3}O_{12}$:0.01$Ce^{3+}$ sample which yields the brightest PersL, using the structural information reported for $Mg_3Y_2Ge_3O_{12}$ as the initial model. The refined structural parameters are listed in Table S1, with the reliability factors of weighted profile R-factor (R_{wp}) and the R factor (R_p) converged to 10.20 and 6.58%, respectively. It is confirmed that the compound crystallizes in a cubic structure with space group $Ia\bar{3}d$ (No. 230) and the cell parameters of $a = b = c = 12.2256$ Å, $V = 1827.31$ Å^3. Compared to those reported in the pure MYGO crystal ($a = b = c = 12.2489$ Å, $V = 1837.77$ Å^3), the decreased cell parameters demonstrates that Si successfully occupies in the Ge site by forming a solid solution. Figure 2b displays the crystal unit cell of the $Mg_3Y_{1.99}Ge_{2.7}Si_{0.3}O_{12}$:0.01$Ce^{3+}$ inverse garnet which comprises three types of coordination polyhedral with the dodecahedral

site occupied by Y^{3+}/one-third of Mg^{2+}, the octahedral site by the rest of Mg^{2+}, and the tetrahedral site by Ge^{4+}/Si^{4+}, respectively. Considering that there are two coordinated sites occupied by two different cationic ions, the local crystalline environment around the active ions Ce^{3+} is complex, and thus, some intriguing luminescent properties would be anticipated.

3.2. Photoluminescence Characteristics. Steady-state luminescent properties of the samples with various Ge/Si ratios were measured in Figure 3a, showing typical Ce^{3+}:5d_1 → 4f
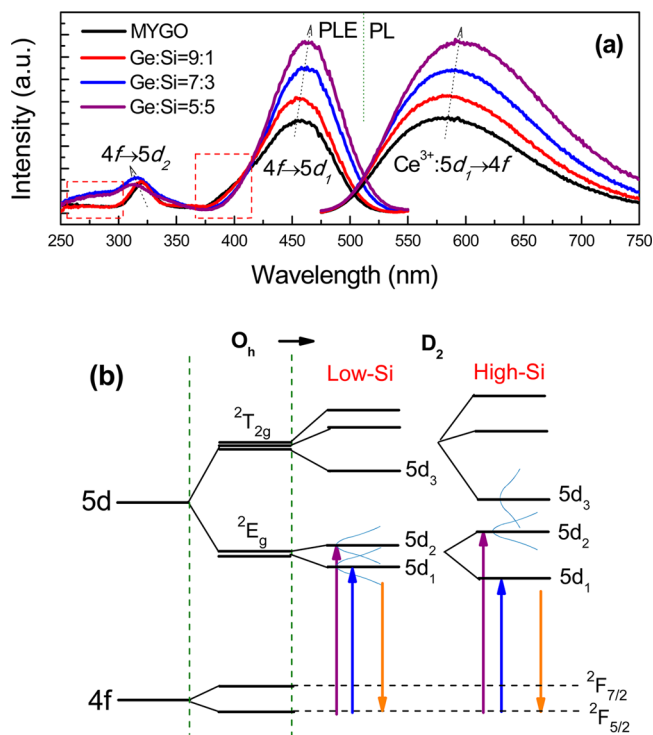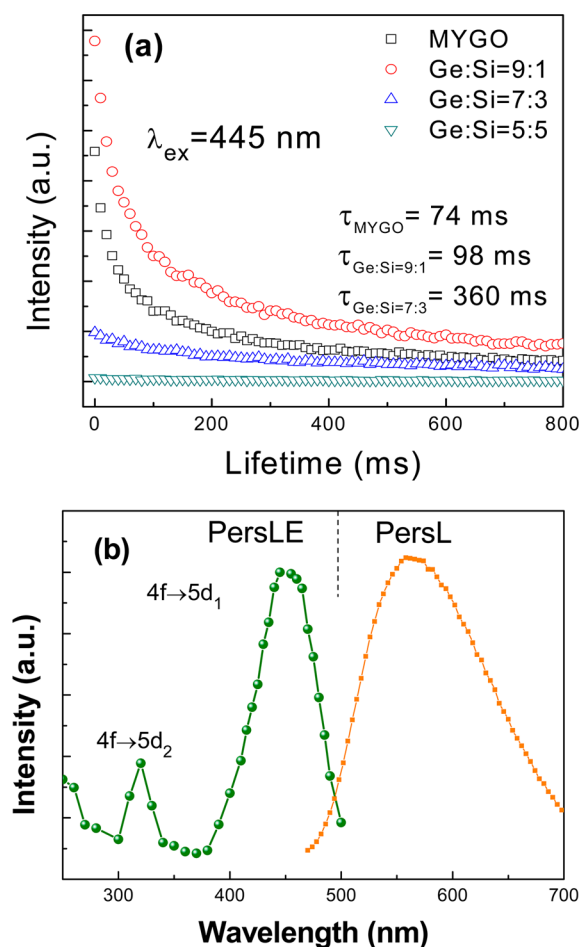

Figure 3. (a) PL and PLE spectra of the samples as a function of Ge/Si ratio. (b) Energy-level diagram showing energy splitting and orbital overlap in low-Si and high-Si samples.

emission band in the photoluminescence (PL) spectra (λ_{ex} = 455 nm) and two Ce^{3+}:4f → 5d_1, 5d_2 excitation bands in the PL excitation (PLE) ones (λ_{em} = 580−595 nm). It is found that the increased Si doping leads to red-shifting of the 4f ↔ 5d_1 peak wavelengths and blue-shifting of the 4f → 5d_2 peak wavelength. Interestingly, the 4f → 5d_1 band broadens toward in the high energy direction in low-Si content samples, whereas such broadness emerges in the 4f → 5d_2 band of high-Si content ones. To explain these phenomena, we should consider the energy splitting of Ce^{3+} ions under the specific crystal field strength of $Mg_3Y_2(Ge_{1-x}Si_x)_3O_{12}$ (x = 0−0.5) inverse garnet. As mentioned above, Ce^{3+} substitutes for Y^{3+} at a dodecahedral site, which shows a local D_2 symmetry. On the basis of group theory, the Ce^{3+}:5d level splits into five sublevels (denoted as 5d_1, 5d_2, ...) when the site symmetry descends from O_h to D_2, as illustrated in Figure 3b. The higher the crystal field strength, the more severe the extent of the energy splitting. The [CeO_8] coordinated polyhedron is constructed with four longer bonds and four shorter ones, which can be viewed as a distorted cube compressed along one axis.[33] There is an increasing compression on the cube by replacing Si for Ge, as demonstrated by Wu et al.,[34] and thus, the enhanced crystal field strength drives the energy splitting of 5d_1 to lower energy

and that of $5d_2$ to higher one. In low-Si case, the splitting is small, so there probably exists an orbital overlap between $5d_1$ and $5d_2$, causing the broadness of $4f \rightarrow 5d_1$ band toward $5d_2$. As the Si content is increased further, the distance between $5d_1$ and $5d_2$ centroids enlarges, and correspondingly, such broadness disappears; instead, the possible orbital overlap between $5d_2$ and $5d_3$ forces $4f \rightarrow 5d_2$ band to shift toward $5d_3$. As for the increased emission intensity, it should be related to the decreased photon loss via photoionization ($5d_1 \rightarrow$ CB).[35,36] The measured QY for the $Mg_{2.99}Y_2(Ge_{1-x}Si_x)_3O_{12}:0.01Ce^{3+}$ (x = 0−0.5) phosphors are presented in Figure S1. As the Si content (x) increases from 0 to 0.5, QY increases correspondingly from 28.8 to 51.1%.
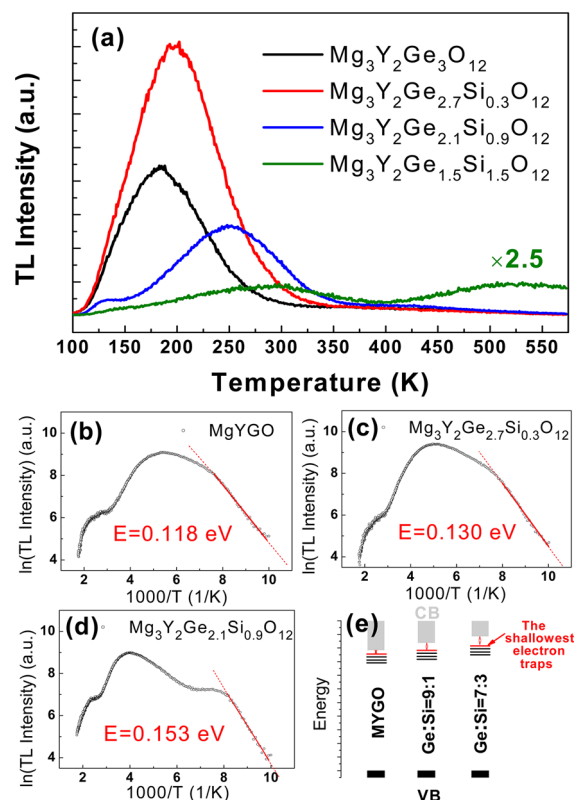
3.3. PersL Characteristics. To evaluate the persistent performance of the $Mg_3Y_{1.99}(Ge_{1-x}Si_x)_3O_{12}:0.01Ce^{3+}$ (x = 0−0.5) samples, we recorded the PersL decays after ceasing the 445 nm excitation at room temperature. Noticeably, all the decays are comprised of a bright, fast component in the millisecond range (Figure 4a) and a weak, slow one up to 30 s clearly observed by the unaided eye in the dark (Figure S2). We were only concerned about the bright fast decay because it is probably able to compensate the dimming time of AC-LED. In the time window of milliseconds, the PersL intensity increases when Si content is added in the MYGO to Ge:Si = 9:1, then

decreases when Si content is increased to Ge:Si = 7:3, and totally disappears when Si is further enriched to Ge:Si = 5:5. The PersL lifetime, estimated by the time of the luminescence decreases to $1/e$ of the initial intensity, is determined elevating from 74 to 360 ms. The explanation for these phenomena is discussed in section 3.5. Figure 4b displays the PersL and PersLE spectra of the sample. The PersL spectral profile is found identical to the PL one, suggesting that the PersL originates from the Ce^{3+} emissive centers. The PersLE spectrum, created by plotting the afterglow intensities at 100 ms (as a reference point) after the stoppage of excitation versus the excitation wavelength (the representative afterglow curve is presented in Figure S3), resembles the PLE spectrum, implying the intense afterglow luminescence should be achieved via efficient Ce^{3+} excitation in the blue region. To achieve the brightest PersL intensity, we have optimized the Ce^{3+} concentration and the flux H_3BO_3 amount to be 0.5 mol % and 4 wt %, as shown in Figure S4.

3.4. Trap Analyses. For better understanding of the Ge/Si ratio dependent PersL behavior, the trap variation should be evaluated in detail. To this end, the thermo-luminescence (TL) technique is adopted for probing the trap properties in the $Mg_3Y_{1.99}(Ge_{1-x}Si_x)_3O_{12}:0.01Ce^{3+}$ (x = 0−0.5) samples. We perform TL measurements starting from the temperature close to nitrogen (100 K) aiming to gain trap information responsible for the millisecond afterglow, as presented in Figure 5a. There is one major broad TL peak centered at 180− 300 K in each sample. Obviously, the TL peak shifts to higher temperature as Ge/Si ratio decreases, indicating the trap depth

Figure 4. (a) Ge/Si ratio dependent PersL decay curves (λ_{ex} = 445 nm, λ_{em} = 580 nm); (b) PersL and PersLE spectra of the $Mg_3Y_{1.99}Ge_{2.7}Si_{0.3}O_{12}:0.01Ce^{3+}$, wherein PersLE curve is plotted with the afterglow intensity $I_{100\ ms}$ monitored at 580 nm as a function of the excitation wavelengths over the 250−500 nm spectral range.


Figure 5. (a) Ge/Si ratio dependent TL curves measured at a heating rate of 1 K/s after 445 nm irradiation for 5 min. (b−d) Initial rise analyses of corresponding TL curves revealing the shallowest occupied traps. (e) Schematic illustration of the variation in the energy band and the trap depth.

gets deeper, since the trap depth is generally proportional to the peak temperature of the PersL curve.[37] Also noteworthy, the TL intensity exhibits an identical variation trend to that in PersL intensity. This is reasonable for that the TL intensity reflects the concentration of carriers stored in the traps.[18] An initial rising method was further applied to the measured TL curves to reveal the shallowest occupied electron trap depth (E), as presented in Figure 5b−d. This method assumes that the concentration of trapped electrons on the low-temperature side of a TL glow curve remains relatively constant, therefore the TL intensity ($I(T)$) should be independent of the TL kinetics and can be approximately expressed as[38−40]

$$I(T) = C \exp\left(\frac{-E}{kT}\right) \tag{1}$$

where C is the constant including the frequency factor s, and k the Boltzmann constant. By plotting the TL curves as $\ln(I)$ versus ($1000/T$), the shallowest trap depth E can be determined by the slope of a fitted straight section at the low-temperature side. The estimated shallowest trap depths for MYGO, $Mg_3Y_2Ge_{2.7}Si_{0.3}O_{12}$, and $Mg_3Y_2Ge_{2.1}Si_{0.9}O_{12}$ samples are as low as 0.118, 0.130, and 0.153 eV, respectively. Such shallow trap depth is believed to be the origin of the millisecond afterglow. The TL signal in $Mg_3Y_2Ge_{1.5}Si_{1.5}O_{12}$ sample is too weak, so the fitted result has errors and is not shown here. It is known that the trap depth corresponds to the energy gap between the electron trap level and the CB bottom. For one specified trap with a fixed energy location, depth certainly increases with the elevation of CB bottom; moreover, the variation extent of depth should be in accordance with that of energy band. In the present case, with decreasing Ge/Si ratio, the shallowest trap depth deepens at a step of ∼0.02 eV, while the energy band of host widens at a step of ∼0.2 eV (bandgaps of the samples are determined by the Kubelka−Munk transformed diffuse reflectance spectra shown in Figure S5), which indicates that the increased Si content forces the shallowest trap level shifting to a higher energy (Figure 5e). Therefore, this trap is not changeless and should not be assigned to the commonly assumed oxygen vacancies (V_O). We inferred that it might be ascribed to Ge-related trap, such as the intrinsic Ge point defect or the $V_{Ge}−Ce^{3+}−V_O$ defect clusters,[17] by considering the trap is strongly influenced by Si doping.

To gain more insight into the trapping and detrapping behaviors involved for the PersL of $Mg_3Y_{1.99}(Ge_{1−x}Si_x)_3O_{12}$:$0.01Ce^{3+}$ (x = 0−0.5), we performed a series of excitation duration and excitation temperature dependent TL experiments on the representative $Mg_3Y_2Ge_{2.7}Si_{0.3}O_{12}$ sample which yields the brightest PersL. Figure 6 presents the measured TL curves by pre-exciting the sample at 445 nm (100 K) for different durations and then recording at a heating rate of 1 K/s. The TL intensity enhances with prolonging the exposure time, due to more electrons are captured by the traps. There is no appreciable shift in the glow peak maximum, suggesting the first-order kinetic, that is, every charge carrier released from a trap immediately produces luminescence, dominates the detrapping process, as described by Randall and Wilkins.[41] The first-order TL curve is featured by an asymmetric glow peak with a negative skew, while in our case, the curve profile is close to symmetric and rather broad. This indicates a possible overlap of various peaks having a close distribution of their trap depths.[42] To distinguish these traps and determine the trap depth distributions, we conducted TL measurements by varying the excitation temperature, as
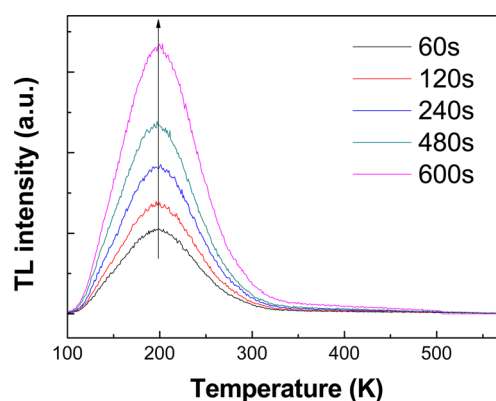
Figure 6. Excitation duration dependent TL glow curves at a heating rate of 1 K/s.

exhibited in Figure 7a. The measurement condition is comparable to the one proposed by Van den Eeckhout et al.[38] For each curve, the sample is cooled/heated to a given excitation temperature (T_{exc}), irradiated by 445 nm light for 5 min, delayed at a time interval of 3 min, and then measured starting from T_{exc} at a heating rate of 1 K/s. The time interval is set up to exclude the influence of fast decay process. The physical picture of applying such approach to validate the trap depth distribution has also been explained by Van den Eeckhout et al.[38] Briefly, the T_{exc} influences the distribution of the trapped electrons in a way by partially detrapping the electrons in the shallower traps, so the TL curves measured at different T_{exc} provide information from the different unemptied fractions of trap, as schematically illustrated in Figure S6. Figure 7b depicts the extracted information from Figure 7a, including the dependence of TL peak temperature (T_{peak}) and TL peak intensity (I_{peak}) on the T_{exc}. Three trap types can be identified by their distinct TL characteristics as the increase of T_{exc}: Trap 1, T_{peak} ↑ (slightly), I_{peak} ↓; Trap 2, T_{peak} ↑, I_{peak} ↓; and Trap 3, T_{peak} ↑, I_{peak} ↑. Evidently, the distribution of Trap 1 is quite narrow, while that of Trap 2 and 3 are rather broad. The increase in T_{peak} is ascribed to that the electrons are distributed into the deeper traps as increasing of T_{exc}. The different variation trend in I_{peak} is believed to be caused by the compromise between two factors—the thermally depleted electrons from traps to CB and the thermally facilitated electron trap fillings via photoionization. The former factor takes control for Traps 1 and 2 because they are relatively shallower and more susceptible to the heat and thus more easily to release the electrons to CB, whereas the latter prevails for Trap 3. The transformed Arrhenius plot for each curve in Figure 7a is shown in Figure 7c. All the plots present a straight section in the low-temperature side, implying that our assumption for the initial rising analysis is valid. From the fitted slopes, we get knowledge of the depths of shallowest occupied traps after thermal-cleaning at different T_{exc}. Obviously, the estimated trap depth gradually deepens from 0.13 to 0.54 eV with increasing the T_{exc}, thus the continuous trap depth distribution is demonstrated (Figure 7d). Interestingly, the T_{exc} versus trap depth plot can be fitted by three different functions, implying that the three traps have different distribution characteristics. Trap 1 follows a linear plot, indicating the detrapping rate is constant, so is considered having a uniform distribution. Trap 2 agrees well with a polynomial fit and thus is probably attributed to a Gaussian
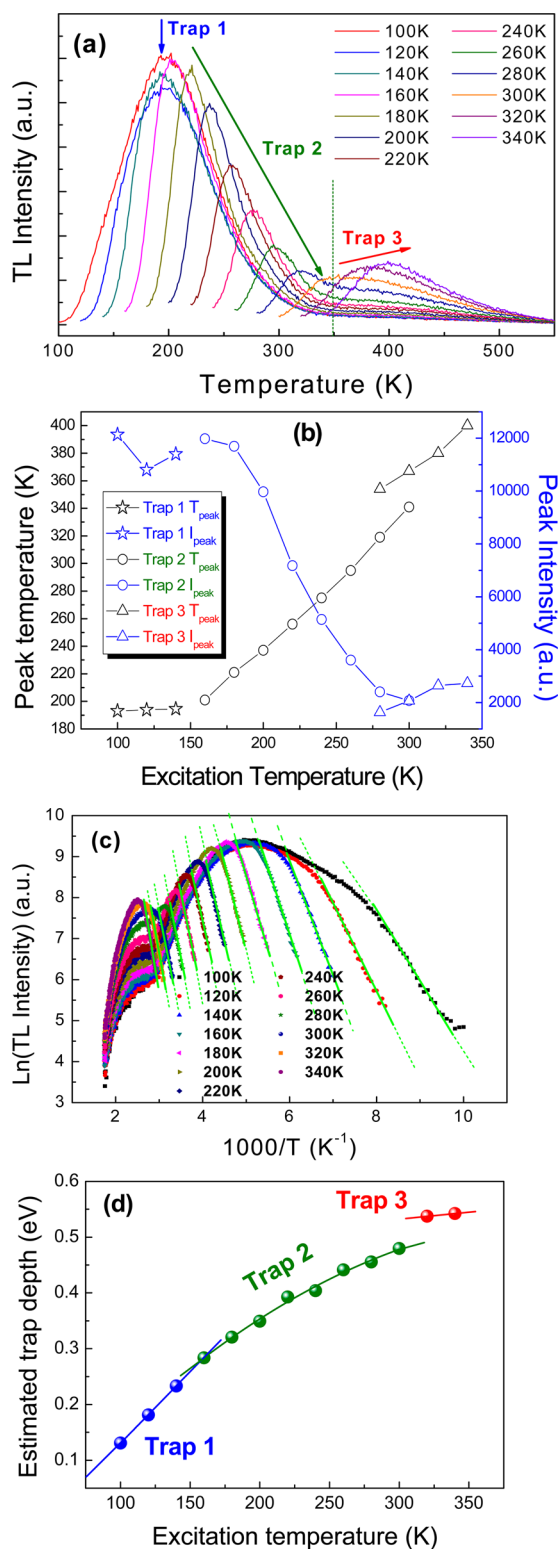
Figure 7. (a) Excitation temperature-dependent TL curves by preheating/cooling the $Mg_3Y_2Ge_{2.7}Si_{0.3}O_{12}$ sample at different T_{exc} (excitation wavelength, 445 nm; heating rate, 1 K/s). (b) Dependence of T_{peak} and I_{peak} on the T_{exc}. (c) Initial rise analyses on all the TL curves as a function of T_{exc}. (d) Estimated trap depth as a function of T_{exc}; the solid lines represent the fit through the data points.

distribution.[38] The recording data for Trap 3 is not enough, but we believe it also follows a Gaussian distribution.

3.5. PersL Mechanism. A possible PersL mechanism for the $Mg_3Y_{1.99}(Ge_{1-x}Si_x)_3O_{12}:0.01Ce^{3+}$ (x = 0−0.5) inverse garnet is proposed, as schematically illustrated in Figure 8, which includes the major processes of ① blue-light excitation, ② electron photoionization from $Ce^{3+}:5d_1$ excited level, ③ electron transmission via CB, ④ electron trapping and detrapping, and ⑤ electron recombination. The generated PersL under blue light excitation follows the sequence of ① → ② → ③ → ④ → ⑤, similar to those reported in the $Ln_3Al_{5-x}Ga_xO_{12}:Ce^{3+}$ (Ln = Y, Gd, Lu; x = 1−4) persistent phosphors.[12,28−32] On the basis of the above results and analyses, we propose that Si doping influences both the electron charging and electron detrapping processes by tailoring the host bandgap. For the MYGO sample, the bandgap is narrowest. The excited $Ce^{3+}:5d_1$ level probably gets too close to the CB bottom, or even overlap with it, so a part of the thermally released electrons from the trap may not combine with the emissive centers, but go back to the traps (retrapping process), consequently the PersL exhibits relatively low brightness. With increasing Si contents, the gap between the excited $Ce^{3+}:5d_1$ level and the CB bottom enlarges so that the retrapping process becomes insignificant (first-order kinetic), therefore the brightest PersL is observed when Ge:Si = 9:1, whereas if the gap is too large, the photoionization process becomes inefficient or even does not occur, so the PersL intensity is very weak when Ge:Si = 7:3 and totally disappears when Ge:Si = 5:5. On the other hand, the trap tends to be deeper with decreasing of Ge/Si ratio, thus the afterglow lifetime prolongs correspondingly. The optimized $Mg_3Y_2Ge_{2.7}Si_{0.3}O_{12}:Ce^{3+}$ sample yields the brightest PersL with a lifetime of 98 ms, which might compensate the dimming time of AC-LED.

3.6. AC-LED Performance. As a proof-of-concept experiment, an AC-LED prototype device was fabricated by coupling the $Mg_3Y_{1.99}Ge_{2.7}Si_{0.3}O_{12}:0.01Ce^{3+}$-based phosphor-in-silicone (PiS, made by dispersing $Mg_3Y_{1.99}Ge_{2.7}Si_{0.3}O_{12}:0.01Ce^{3+}$ phosphor in silicone in a weight ratio of 5:1) with a commercial InGaN blue-emitting chip, and connected to an AC bridge circuit (Figure S7). Figure 9a displays the PiS thickness dependent electroluminescent (EL) spectra of the fabricated AC-LEDs by normalizing all the spectra to blue emission band of the chip. As expected, Ce^{3+} emission enhances with increasing of the thickness caused by the longer interaction pathway between the blue light and the phosphor. Correspondingly, the CIE chromaticity coordinates can be adjusted to following the line across the CIE coordinate point of the blue chip (0.154, 0.027) and that of the $Mg_3Y_2Ge_{2.7}Si_{0.3}O_{12}:Ce^{3+}$ phosphor (0.4916,0.4948), as exhibited in Figure 9b. Therein, point 3 produces warm white light with a CIE coordinate of (0.4264, 0.4072) just located on the Planckian locus, a correlated color temperature (CCT) of 3211 K, and a color rendering index of 75.8. To evaluate the feasibility of $Mg_3Y_{1.99}Ge_{2.7}Si_{0.3}O_{12}:0.01Ce^{3+}$ PersL phosphor for reducing the flickering effect, we measured EL intensity variation of AC-LED with and without the $Mg_3Y_{1.99}Ge_{2.7}Si_{0.3}O_{12}:0.01Ce^{3+}$ based PiS under AC periodic cycles, as presented in Figure 9c. The percent flicker (δ), expressed as $\delta = ((I_{max} - I_{min})/(I_{max} + I_{min})) \times 100$,[43] reflects the flickering effect, where I_{max} and I_{min} represent the maximal and minimal luminescent intensity. Remarkably, the percent flicker reduces from 100 to 71.7% thanking to the dimming time compensation by the PersL.
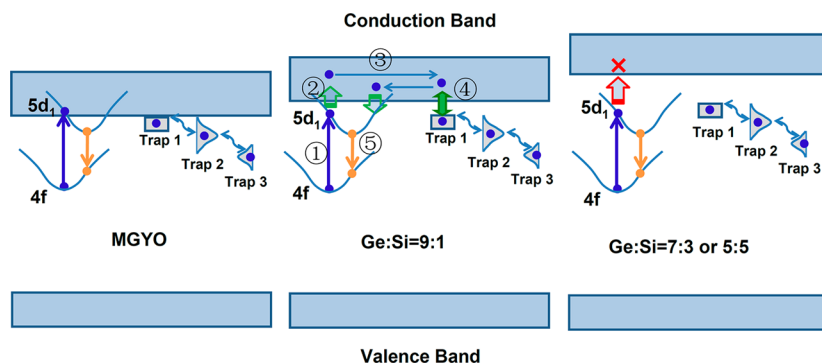
Figure 8. Schematic illustration of the Ge/Si ratio dependent PersL mechanism.
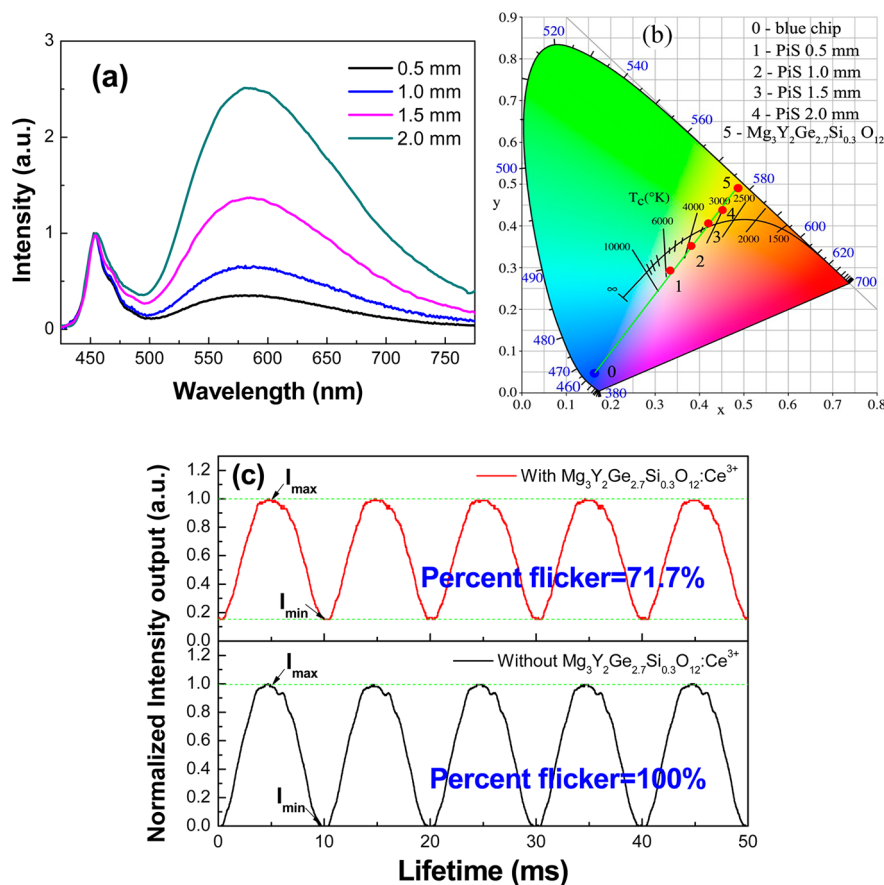

Figure 9. (a) Electroluminescent spectra and (b) CIE chromaticity points of the fabricated AC-LEDs by varying the PiS thickness. (c) Luminescence intensity variation of the warm w-LEDs with and without the $Mg_3Y_{1.99}Ge_{2.7}Si_{0.3}O_{12}:0.01Ce^{3+}$ based PiS driven in AC periodic cycles.

4. CONCLUSIONS

In summary, we developed a novel PersL phosphor $Mg_3Y_{1.99}(Ge_{1-x}Si_x)_3O_{12}:0.01Ce^{3+}$ ($x = 0-0.5$) pure-phase solid solution using a high-temperature solid-state sintering method. When the Ge/Si ratio varies, the PL behavior of the sample greatly alters, which is ascribed to the different extents of energy splitting caused by the change in crystal field strength of the host. Interestingly, the samples yield orange emissive PersL in the millisecond time window under blue-light activation, wherein $Mg_3Y_{1.99}Ge_{2.7}Si_{0.3}O_{12}:0.01Ce^{3+}$ exhibits brightest PersL with a decay lifetime of 98 ms. We demonstrated that an appropriate energy gap between the excited Ce^{3+}:5d level and the CB bottom is of vital importance to achieve blue-light activated PersL: if it is too narrow or

overlaps with CB, then the adverse electron retrapping might become significant; if it is too large, then electron photoionization would not occur. For the $Mg_3Y_{1.99}Ge_{2.7}Si_{0.3}O_{12}:0.01Ce^{3+}$, it is confirmed that the host contains three trap types with a continuous trap depth distribution varying from 0.13 to 0.54 eV. The shallowest trap might be responsible for the origin of the millisecond afterglow. Furthermore, $Mg_3Y_{1.99}Ge_{2.7}Si_{0.3}O_{12}:0.01Ce^{3+}$-based AC-LED prototype device was fabricated to validate its ability to compensate AC flickering effect. The optimized device yields warm white light with a CIE coordinate of (0.4264, 0.4072) just located on the Planckian locus, a correlated color temperature (CCT) of 3211 K, a color rendering index of 75.8, and a reduced percent flicker of 71.7%.

■ ASSOCIATED CONTENT

ⓈSupporting Information

The Supporting Information is available free of charge on the ACS Publications website at DOI: 10.1021/acsami.5b06071.

The refined positions of all atoms and the lattice parameters of $Mg_3Y_2Ge_{2.7}Si_{0.3}O_{12}:Ce^{3+}$. QY measurement for the $Mg_{2.99}Y_2(Ge_{1-x}Si_x)_3O_{12}:0.01Ce^{3+}$ ($x = 0-0.5$) phosphors (Figure S1). The Ge/Si ratio dependent afterglow curves recorded in the time window of 1 min. The representative afterglow curves versus the excitation wavelength. The PersL decay curves for the $Mg_3Y_{2-x}Ge_{2.7}Si_{0.3}O_{12}:xCe^{3+}$ phosphor ($x = 0.005-0.04$) and the H_3BO_3 amount (0−6 wt %). Kubelka−Munk transformed diffuse reflectance spectra for determination of the host bandgap (E_g) by plotting $[F(R)h\nu]^2$ versus photon energy $h\nu$, where R is the reflectance, and $F(R)$ is the Kubelka−Munk function ($F(R) = (1 - R)^2/2R$). A tangent line is drawn in the near edge region of the curve. The $h\nu$ value at the crossing point of the tangent line and the horizontal axis represents the band gap. The physical picture of applying the T_{exc} dependent TL curve approach to evaluate the trap depth distribution. A homemade AC-LED prototype device in operation. (PDF)

■ AUTHOR INFORMATION

Corresponding Author
*E-mail: yswang@fjirsm.ac.cn. Tel/Fax: +86-591-83705402.

Notes
The authors declare no competing financial interest.

■ ACKNOWLEDGMENTS

■ REFERENCES

(1) Ye, S.; Xiao, F.; Pan, Y. X.; Ma, Y. Y.; Zhang, Q. Y. Phosphors in Phosphor-Converted White Light-Emitting Diodes: Recent Advances in Materials, Techniques and Properties. *Mater. Sci. Eng., R* 2010, 71, 1−34.

(2) Yen, H. H.; Yeh, W. Y.; Kuo, H. C. GaN Alternating Current Light-emitting Device. *Phys. Status Solidi A* 2007, 204, 2077−2081.

(3) Onushkin, G. A.; Lee, Y. J.; Yang, J. J.; Kim, H. K.; Son, J. K.; Park, G. H.; Park, Y. J. Efficient Alternating Current Operated White Light-Emitting Diode Chip. *IEEE Photonics Technol. Lett.* 2009, 21, 33−35.

(4) Cho, J.; Jung, J.; Chae, J. H.; Kim, H.; Kim, H.; Lee, J. W.; Yoon, S.; Sone, C.; Jang, T.; Park, Y.; Yoon, E. Alternating-current Light Emitting Diodes with a Diode Bridge Circuitry. *Jpn. J. Appl. Phys.* 2007, 46, L1194−L1196.

(5) Yen, H. H.; Kuo, H. C.; Yeh, W. Y. Characteristics of Single-Chip GaN-Based Alternating Current Light-Emitting Diode. *Jpn. J. Appl. Phys.* 2008, 47, 8808−8810.

(6) Zhang, R.; Lin, H.; Yu, Y. L.; Chen, D. Q.; Xu, J.; Wang, Y. S. A New-Generation Color Converter for High-Power White LED: Transparent Ce^{3+}: YAG Phosphor-in-Glass. *Laser Photonics Rev.* 2014, 8, 158−164.

(7) Lin, H.; Zhang, R.; Chen, D. Q.; Yu, Y. L.; Yang, A. P.; Wang, Y. S. Tuning of Multicolor Emissions in Glass Ceramics Containing γ-Ga_2O_3 and β-YF_3 Nanocrystals. *J. Mater. Chem. C* 2013, 1, 1804−1811.

(8) Zhang, X. J.; Huang, L.; Pan, F. J.; Wu, M. M.; Wang, J.; Chen, Y.; Su, Q. Highly Thermally Stable Single-Component White-Emitting Silicate Glass for Organic-Resin-Free White-Light-Emitting Diodes. *ACS Appl. Mater. Interfaces* 2014, 6, 2709−2717.

(9) Yeh, C. W.; Li, Y.; Wang, J.; Liu, R. S. Appropriate Green Phosphor of $SrSi_2O_2N_2$: Eu^{2+}, Mn^{2+} for AC LEDs. *Opt. Express* 2012, 20, 18031−18034.

(10) Chen, L.; Zhang, Y. S.; Xue, C.; Deng, X. R.; Luo, A. Q.; Liu, F. Y.; Jiang, Y. The Green Phosphor $SrAl_2O_4$: Eu^{2+}, R^{3+} (R = Y, Dy) and Its Application in Alternating Current Light-Emitting Diodes. *Funct. Mater. Lett.* 2013, 6, 1350047.

(11) Chen, L.; Zhang, Y.; Liu, F. Y.; Luo, A. Q.; Chen, Z. X.; Jiang, Y.; Chen, S. F.; Liu, R. S. A New Green Phosphor of $SrAl_2O_4$: Eu^{2+}, Ce^{3+}, Li^+ for Alternating Current Driven Light-Emitting Diodes. *Mater. Res. Bull.* 2012, 47, 4071−4075.

(12) Lin, H.; Wang, B.; Xu, J.; Zhang, R.; Chen, H.; Yu, Y. L.; Wang, Y. S. Phosphor-in-Glass for High-Powered Remote-Type White AC-LED. *ACS Appl. Mater. Interfaces* 2014, 6, 21264−21269.

(13) Tan, J. C.; Narendran, N. Defining Phosphor Luminescence Property Requirements for White AC LED Flicker Reduction. *J. Lumin.* 2015, 167, 21−26.

(14) Su, Q.; Li, C. Y.; Wang, J. Some Interesting Phenomena in The Study of Rare Earth Long Lasting Phosphors. *Opt. Mater.* 2014, 36, 1894−1900.

(15) IEEE PAR 1789 report, 2010. "Recommending Practices for Modulating Current in High Brightness LEDs for Mitigating Health Risks to Viewers" at: http://grouper.ieee.org/groups/1789/public.html.

(16) Matsuzawa, T.; Aoki, Y.; Takeuchi, N.; Murayama, Y. New Long Phosphorescent Phosphor with High Brightness, $SrAl_2O_4:Eu^{2+}, Dy^{3+}$. *J. Electrochem. Soc.* 1996, 143, 2670−2673.

(17) Pan, Z. W.; Lu, Y. Y.; Liu, F. Sunlight-Activated Long-Persistent Luminescence in The Near-Infrared from Cr^{3+}-Doped Zinc Gallogermanates. *Nat. Mater.* 2011, 11, 58−63.

(18) Van den Eeckhout, K.; Smet, P. F.; Poelman, D. Persistent Luminescence in Eu^{2+}-Doped Compounds: A Review. *Materials* 2010, 3, 2536−2566.

(19) Jin, Y. H.; Hu, Y. H.; Chen, L.; Wang, X. J.; Mou, Z. F.; Ju, G. F.; Liang, F. Luminescent Properties of a Reddish Orange Emitting Long-lasting Phosphor CaO: Pr^{3+}. *Mater. Sci. Eng., B* 2013, 178, 1205−1211.

(20) Li, Y.; Zhou, S. F.; Li, Y. Y.; Sharafudeen, K.; Ma, Z. J.; Dong, G. P.; Peng, M. Y.; Qiu, J. R. Long Persistent and Photo-stimulated Luminescence in Cr^{3+}-Doped Zn-Ga-Sn-O Phosphors for Deep and Reproducible Tissue Imaging. *J. Mater. Chem. C* 2014, 2, 2657−2663.

(21) Zeng, W.; Wang, Y. H.; Han, S. C.; Chen, W. B.; Li, G.; Wang, Y. Z.; Wen, Y. Design, Synthesis and Characterization of a Novel Yellow Long-Persistent Phosphor: $Ca_2BO_3Cl:Eu^{2+}, Dy^{3+}$. *J. Mater. Chem. C* 2013, 1, 3004−3011.

(22) Garlick, G. F. J.; Wilkins, M. H. F. Short Period Phosphorescence and Electron Traps. *Proc. R. Soc. London, Ser. A* 1945, 184, 408−433.

(23) Kanai, T.; Satoh, M.; Miura, I. Characteristics of a Non-stoichiometric $Gd_{3+\delta}(Al,Ga)_{5-\delta}O_{12}:Ce$ Garnet Scintillator. *J. Am. Ceram. Soc.* 2008, 91, 456−462.

(24) Dorenbos, P. Mechanism of Persistent Luminescence in Eu^{2+} and Dy^{3+} Codoped Aluminate and Silicate Compounds. *J. Electrochem. Soc.* 2005, 152, H107−H110.

(25) Jia, D. D.; Wang, X. J.; Yen, W. M. Delocalization, Thermal Ionization, and Energy Transfer in Singly Doped and Codoped $CaAl_4O_7$ and Y_2O_3. *Phys. Rev. B: Condens. Matter Mater. Phys.* 2004, 69, 235113.

(26) Li, Y.; Li, B. H.; Ni, C. C.; Yuan, S. X.; Wang, J.; Tang, Q.; Su, Q. Synthesis, Persistent Luminescence, and Thermoluminescence Properties of Yellow $Sr_3SiO_5:Eu^{2+},RE^{3+}$ (RE = Ce, Nd, Dy, Ho, Er, Tm, Yb) and Orange-Red $Sr_{3-x}Ba_xSiO_5:Eu^{2+}, Dy^{3+}$ Phosphor. *Chem. - Asian J.* 2014, 9, 494−499.

(27) Rodriguez Burbano, D. C.; Sharma, S. K.; Dorenbos, P.; Viana, B.; Capobianco, J. A. Persistent and Photostimulated Red Emission in $CaS:Eu^{2+},Dy^{3+}$ Nanophosphors. *Adv. Opt. Mater.* 2015, 3, 551−557.

(28) Ueda, J.; Kuroishi, K.; Tanabe, S. Bright Persistent Ceramic Phosphors of Ce^{3+}-Cr^{3+}-Codoped Garnet Able to Store by Blue Light. *Appl. Phys. Lett.* **2014**, *104*, 101904.

(29) Ueda, J.; Tanabe, S.; Nakanishi, T. Analysis of Ce^{3+} Luminescence Quenching in Solid Solutions between $Y_3Al_5O_{12}$ and $Y_3Ga_5O_{12}$ by Temperature Dependence of Photoconductivity Measurement. *J. Appl. Phys.* **2011**, *110*, 053102.

(30) Ueda, J.; Kuroishi, K.; Tanabe, S. Yellow Persistent Luminescence in Ce^{3+}-Cr^{3+}-Codoped Gadolinium Aluminum Gallium Garnet Transparent Ceramics after Blue-Light Excitation. *Appl. Phys. Express* **2014**, *7*, 062201.

(31) Ueda, J.; Dorenbos, P.; Bos; Adrie, J. J.; Kuroishi, K.; Tanabe, S. Control of Electron Transfer between Ce^{3+} And Cr^{3+} in the $Y_3Al_{5-x}Ga_xO_{12}$ Host via Conduction Band Engineering. *J. Mater. Chem. C* **2015**, *3*, 5642−5651.

(32) Wang, B.; Lin, H.; Yu, Y. L.; Chen, D. Q.; Zhang, R.; Xu, J.; Wang, Y. S. Ce^{3+}/Pr^{3+}: YAGG: A Long Persistent Phosphor Activated by Blue-Light. *J. Am. Ceram. Soc.* **2014**, *97*, 2539−2545.

(33) Robbins, D. J. The Effects of Crystal Field and Temperature on The Photoluminescence Excitation Efficiency of Ce^{3+} in YAG. *J. Electrochem. Soc.* **1979**, *126*, 1550−1555.

(34) Wu, J. L.; Gundiah, G.; Cheetham, A. K. Structure−Property Correlations in Ce-Doped Garnet Phosphors for Use in Solid State Lighting. *Chem. Phys. Lett.* **2007**, *441*, 250−254.

(35) Jiang, Z. Q.; Wang, Y. H.; Wang, L. S. Enhanced Yellow-to-Orange Emission of Si-Doped $Mg_3Y_2Ge_3O_{12}$:Ce^{3+} Garnet Phosphors for Warm White Light-Emitting Diodes. *J. Electrochem. Soc.* **2010**, *157*, J155−J158.

(36) Shimizu, T.; Ueda, J.; Tanabe, S. Optical and Optoelectronic Properties of Ce^{3+} Doped $Mg_3Y_2(Ge,Si)_3O_{12}$ Inverse Garnet. *Phys. Status Solidi C* **2012**, *9*, 2296−2299.

(37) Aitasalo, T.; Hölsä, J.; Jungner, H.; Lastusaari, M.; Niittykoski, J. Thermoluminescence Study of Persistent Luminescence Materials: Eu^{2+}- and R^{3+}-Doped Calcium Aluminates, $CaAl_2O_4$: Eu^{2+},R^{3+}. *J. Phys. Chem. B* **2006**, *110*, 4589−4598.

(38) Van den Eeckhout, K.; Bos, A. J. J.; Poelman, D.; Smet, P. F. Revealing Trap Depth Distributions in Persistent Phosphors. *Phys. Rev. B: Condens. Matter Mater. Phys.* **2013**, *87*, 045126.

(39) Thermoluminescence of Solids; McKeever, S. W. S., Eds.; Cambridge University Press: Cambridge, U.K., 1985; Chapter 3, pp 64−115.

(40) Bos, A. J. J. Theory of Thermoluminescence. *Radiat. Meas.* **2006**, *41*, S45−S56.

(41) Randall, J. T.; Wilkins, M. H. F. Phosphorescence and Electron Traps. I. The Study of Trap Distributions. *Proc. R. Soc. London, Ser. A* **1945**, *184*, 366−389.

(42) Pitale, S. S.; Sharma, S. K.; Dubey, R. N.; Qureshi, M. S.; Malik, M. M. TL and PL Studies on Defect-Assisted Green Luminescence from Doped Strontium Sulfide Phosphor. *J. Lumin.* **2008**, *128*, 1587−1594.

(43) Illuminating Engineering Society of North America. In *The IESNA Lighting Handbook*, 9th ed.; Rea, M. S., Eds.; Illuminating Engineering Society, New York, 2000; Chapter 2, pp 44−87.